RSC Applied Polymers

ROYAL SOCIETY OF CHEMISTRY

PAPER

View Article Online
View Journal | View Issue

Cite this: *RSC Appl. Polym.*, 2025, **3**, 643

Highly facilitated permeation and enrichment of oxygen from air through a polyvinylimidazole membrane ligated with cobaltporphyrin that kinetically interacts with oxygen†

Hiromi Shinohara, *‡ Hirotsugu Araihara and Hiroyuki Nishide *

A dense and tough membrane of cobalt tetraphenylporphyrin (CoTPP) and poly(1-vinylimidazole-*co*-octyl methacrylate) (OIm) is prepared on a porous support. The oxygen permeability coefficient and oxygen/nitrogen permselectivity reach 10 Barrer and >110, respectively, at a pressure difference between the feed side and permeate side of 2 cmHg. The membrane with a diameter of 10 cm enriches oxygen from dried air to an oxygen concentration >60% through a one-shot permeation process. The reversible but kinetically very active interaction between oxygen molecules and the CoTPP fixed in the OIm membrane is analyzed while the membrane is under high oxygen pressure or low temperature using spectroscopy techniques including laser-flash photolysis: *i.e.* 920 cmHg for the half of the CoTPP interacted with oxygen and extremely rapid oxygen-releasing rate constant of approximately 10^6 s^{-1}, when extrapolated at room temperature. The enhanced oxygen diffusivity is discussed for the oxygen permeation facilitated through the membrane.

Received 11th November 2024,
Accepted 21st February 2025

DOI: 10.1039/d4lp00336e

rsc.li/rscapplpolym

1. Introduction

Polymer membrane-based gas separation has been extensively investigated because of its energy-efficient and low-cost processes with simple and high scalability.[1–5] Practical examples of dense polymer membranes are those composed of aromatic polyimides, polyethersulfones, and poly(vinylidene fluoride)s. Small gaseous molecule separation from mixed gases is based on the diffusivity of the permeate molecules facilitated by differences in molecular diameter. The separation of hydrogen from its mixed gases, including a hydrogen/oxygen mixture produced by water splitting, has been recently highlighted.[6,7] In contrast, the separation of condensed gases, such as carbon dioxide and nitrogen oxides, is mainly driven by the difference in gas solubility into the dense polymer membranes to achieve high permeability and permselectivity.

To separate gaseous molecules with similar physical characteristics, such as boiling point and molecular size, the properties of polymer membranes, including glass transition temperature (T_g) or free volume, are predominant in the development of gas permeation.[8] For example, siloxane rubber is applied as a membrane for oxygen separation from air. However, the permselectivity of oxygen to nitrogen (P_{O_2}/P_{N_2}) remains as low as 2.[9] In a progress article, Koros *et al.* recently reported that a semirigid polymer mimicking the rigid ultramicropore windows of molecular sieves and zeolites is promising for its high permselectivity of P_{O_2}/P_{N_2}.[10] Even in the case of poly(1-trimethylsilyl-1-propyne),[11] which has a rigid main chain and bulky side chain, its P_{O_2}/P_{N_2} remained low, at 2–4, which suggests that it is difficult to attain high permselectivity when designing the molecular structures of polymers.

From another perspective, carrier-mediated transport or facilitated transport has often been investigated as a permselective membrane procedure.[12–14] The International Union of Pure and Applied Chemistry defines the "facilitated transport" process as that when chemically distinct carrier species bind with a specific component in the feedstream, thereby increasing the permeation of this component relative to other components.[15] Facilitated transport with the carrier fixed into a dense membrane has been investigated to separate gaseous molecules, including oxygen from nitrogen.[16,17] The carrier species are immobilized in the polymer membrane by maintaining their specific binding capability. Various carrier species to selectively bind and separate gaseous molecules have been reported. Representative species are cobalt(II) picket-fence porphyrins[18–20] with a cavity structure as a specific site for oxygen coordination and cobalt(II) salcomines,[21,22] which

Research Institute for Science and Engineering, Waseda University, Tokyo 169-8555, Japan. E-mail: hiromi.shinohara@aoni.waseda.jp, nishide@waseda.jp

†Electronic supplementary information (ESI) available. See DOI: https://doi.org/10.1039/d4lp00336e

‡Present address: National Institute of Technology, Toyota College, Aichi 471-8525, Japan.

selectively bind molecular oxygen from air at room temperature. Another carrier species is monovalent silver (Ag^+) salts, which interact with olefins from olefin/paraffin[23–27] and carbon monoxide from carbon monoxide/nitrogen[28] mixtures. These carriers, when fixed in the polymer matrix, strongly bind the specific gaseous molecules to solubilize them within the membrane and yield a concentration gradient of the specific molecule as a driving force for selective permeation. The facilitated oxygen transport process was successfully analyzed as being a dual-mode transport model,[16,17] *i.e.*, linear combination of the contribution of Langmuir-type adsorption of the specific molecule and physical permeation of the feed species.

In addition, simple, unmodified, and planar cobalt porphyrins and phthalocyanines have been reported as fixed carriers for oxygen separation membranes.[29–36] However, the oxygen-binding capability of these simple cobalt porphyrins and phthalocyanines has not been recognized in inorganic and coordination chemistry,[37,38] and, at least, the capability has not been verified under the conditions of permeation experiments. Moreover, the incorporation of the carrier molecules in the membrane influenced the physical properties of the membrane in some of these previous studies, which might make the permeation results unclear. Furthermore, the oxygen and nitrogen permeabilities were measured with single-gas permeation experiments in these previous studies. The feasibility of the reported permselectivity is uncertain for practical separation of oxygen and nitrogen mixed gases or, ultimately, air.

In this study, a dense and tough membrane was successfully prepared using a simple, planar, and cavity-free cobalt(II) tetraphenylporphyrin (CoTPP) as a fixed carrier and poly(vinylimidazole-*co*-octyl methacrylate) (OIm) as a polymer ligand. The ligation of the imidazole moiety of OIm to the cobalt(II) ion forms a five-coordinated CoTPP, of which the sixth coordination site is vacant to possibly interact with an oxygen molecule. To optimize the balance between the imidazole moiety content and membrane formability, an octyl group was selected as the alkyl group of the methacrylate in this study and the imidazole moiety content of OIm was determined to be 30 wt%. This allowed for the ligation of the imidazole moiety even at high CoTPP concentrations and enabled the membrane to withstand permeation measurements at elevated pressures. The membrane was carefully coated on a porous support with nanometer thickness, and the obtained immobilized membrane was applicable to the feed side under high pressure and easily scaled up to a large area. In addition, the physical properties of the CoTPP-incorporated membranes were maintained at the same rubbery state, including a constant T_g with a constant physical nitrogen permeability coefficient, to quantitatively examine and clearly study the permeation results obtained with different membrane sizes and conditions. A membrane with diameter of 10 cm was fabricated and oxygen enrichment from dried air through a single-shot permeation process was demonstrated using a custom-made permeation apparatus. To discuss the function of the simple and planar CoTPP fixed in the OIm membrane in terms of oxygen permselectivity, the interaction of the CoTPP with oxygen was, for the first time, studied with rapid-reaction spectroscopy and measurements under high oxygen pressure. The mechanism of the oxygen-facilitated permeation with the simple CoTPP fixed in the OIm membrane is discussed from the perspective of the kinetically very active fixed carrier.

2. Experimental section

2.1. Materials

Cobalt(II) tetraphenylporphyrin (CoTPP) was purchased from Sigma-Aldrich. Cobalt(II) *meso*-α,α,α,α-tetrakis(*o*-pivalamidophenyl)porphyrin (CoTpivPP) was synthesized as previously described.[39,40] A polyacrylonitrile ultrafiltration membrane, obtained from GMT Membranetechnik, was selected (see the ESI†) as a porous support. 1-Vinylimidazole and octyl methacrylate were purchased from TCI and used after purification by distillation, with boiling points of 80 °C/4 mmHg and 65 °C/15 mmHg, respectively. Other solvents were purchased from Kanto Chem. and distilled prior to use.

Poly(1-vinylimidazole-*co*-octyl methacrylate) (OIm) was prepared *via* radical copolymerization. 1-Vinylimidazole (30 mL, 0.12 mol) and octyl methacrylate (42 mL, 0.18 mol) were added to a mixed solution of toluene (72 mL) and ethanol (48 mL) under a nitrogen atmosphere and reacted at 65 °C for 4 h with 2,2′-azobisisobutyronitrile (TCI, 0.06 mg, 37 mmol) as an initiator. The reaction mixture was poured into a large excess of methanol, and the precipitate was dissolved in a small amount of toluene and re-precipitated into methanol to obtain poly(1-vinylimidazole-*co*-octyl methacrylate) (24 g, 35%) with a molecular weight of 1.3×10^5 with M_w/M_n = 1.8, and imidazole moiety content of 30 mol%, which were determined by gel permeation chromatography and elemental analysis, respectively.

2.2. Membrane preparation

OIm (3.7 mg) was thoroughly dissolved in THF (0.5 mL) overnight in a nitrogen-filled glove box. CoTPP (2.8 mg) was added and mixed to obtain the CoTPP–OIm solution. The solution was passed through a PTFE membrane filter (Whatman Puradisc) with a pore size of 0.1 μm. The filtered solution was placed on a polyacrylonitrile porous support, carefully spread with a closely wound K bar (#0, wet film deposit height = 4 μm) in a glovebox using a K hand coater (RK PrintCoat Instruments), and kept for 1 h under a nitrogen atmosphere. The membrane was then completely dried under vacuum to obtain the CoTPP–OIm-coated membrane.

2.3. Permeation measurement for a single gas

The volumetric gas flow rates of oxygen and nitrogen at various feed gas pressures were measured using a self-made permeation apparatus with a soap-bubble flowmeter, as shown in Fig. S1.† The range of the feed pressure (p) was 77–196 cmHg, while the pressure of the permeate side was

atmospheric pressure. The pressure difference between the feed and permeate sides is expressed as $(\Delta p) = p$ −atmospheric pressure (76 cmHg). The permeability coefficient (P) was calculated from the volume of permeate (Q) and membrane thickness (l) obtained from the SEM image using eqn (1):

$$P = (Q \cdot l)/(\Delta p \cdot A \cdot t) \quad (1)$$

where A is the active area of the membrane and t is the time to obtain Q.

2.4. Permeation measurement for dried air (mixed oxygen/nitrogen gas)

The oxygen concentration on the permeate side was monitored by gas chromatography (Shimadzu GC-14B) using a gas sampler (10 mL) and He as the sweep gas (flow rate: 40 mL min^{-1}).

2.5. Oxygen permeability and enrichment from dry air using enlarged CoTPP–OIm membranes

A self-made gas permeation apparatus for a larger membrane (10 cm diameter) was assembled to measure the permeation volume with either a soap-bubble flowmeter or a flowmeter (Agilent ADM2000), while the oxygen concentration was measured using a fluorescence oxygen analyzer (ASR F0-960). Dried air was used as the carrier gas.

2.6. Spectroscopic measurements

The interaction of oxygen with the CoTPP complexed with OIm was measured spectroscopically using a UV-vis spectrophotometer (V-550, JASCO) on the membrane cast on either the quartz window for the high-pressure cell or the quartz plate for the low-temperature measurement, with a thickness of approximately 1 μm. The oxygen binding kinetics was studied with a pulsed laser-flash spectrophotometer (FR-2000, Unisoku). The ESR spectrum of the deoxygenated CoTPP–OIm membrane was monitored with a JES-TE200ERS spectrophotometer (JEOL). A small piece of the dense membrane was packed in a quartz glass tube under an oxygen-free atmosphere at −77 K.

2.7. Other measurements

The cross-sectional view of the CoTPP–OIm membrane was measured using FE-SEM (JEOL S-2500CX, acceleration voltage: 25 kV). The surface topography of the CoTPP–OIm membrane was monitored using AFM (Veeco Nanoscope IIIa) in tapping-mode. The T_g of the membrane was measured using differential scanning calorimetry (Seiko Instruments SSG/560U).

3. Results and discussion

3.1. Membrane of the cobaltporphyrin-ligated polyvinylimidazole and highly selective oxygen permeation

Membranes were prepared by coating the tetrahydrofuran solution of OIm and CoTPP upon a porous support, as illustrated in Fig. 1. A molar ratio of [imidazole moiety]/[CoTPP] = 1.67 : 1 (= 42 wt% in CoTPP–OIm) and OIm concentration in the coating solution of 0.9 wt% were carefully selected to effectively ligate the imidazole moiety to CoTPP and avoid soaking the CoTPP–OIm in the pores of the supporting membrane using a bar coater, respectively (see ESI, Table S1 and Fig. S2†). The CoTPP–OIm-coated membrane was homogeneously light brown in color. Surface scanning electron microscopy (SEM) and atomic force microscopy (AFM) images supported the formation of a smooth and pinholeless membrane. The cross-sectional SEM images indicate dense membrane formation with a thickness of approximately 80 nm on the porous support without filling the pores in the porous support. The membrane was mechanically robust, and the dense CoTPP–OIm membrane did not peel off or crack, even under high-pressure application during permeation measurements.

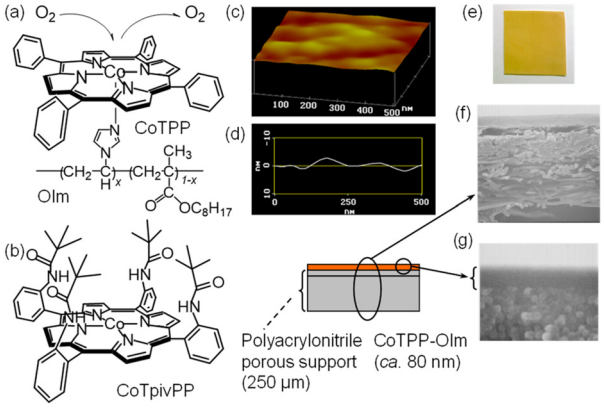

Fig. 1 Chemical structures of (a) cobalt tetraphenylporphyrin (CoTPP) and poly(vinylimidazole-*co*-octyl methacrylate) (OIm), and (b) cobalt *meso*-tetra(*α,α,α,α*-*o*-pivalamidophenyl)porphyrin (CoTpivPP). (c) and (d) Atomic force microscopy images of the CoTPP–OIm membrane on a porous support. (e) Photograph of the CoTPP–OIm membrane on the porous support. (f) and (g) Cross-sectional scanning electron microscopy images of the CoTPP–OIm membrane.

To provide a series of CoTPP–OIm membranes with similar physical properties, including glass transition temperature (T_g) and nitrogen permeability coefficient (P_{N_2}), the total CoTPP concentration incorporated into the OIm membrane was tuned to a constant value of 42 wt%, by mixing Co^{II}TPP, which interacts with molecular oxygen reversibly, with Co^{III}TPP, which does not interact with or is inactive toward oxygen (Co^{II}TPP + Co^{III}TPP = constant 42 wt% in the membrane). T_g and P_{N_2} values of the CoTPP–OIm membranes were maintained at approximately 6.0 °C and 0.09 Barrer (1 Barrer = 10^{-10} cm^3 (STP) cm cm^{-2} s^{-1} $cmHg^{-1}$, which is 3.35×10^{-16} mol m m^{-2} s^{-1} Pa^{-1} in SI units), respectively. The membrane thicknesses, T_g values, and P_{N_2} values of the series of CoTPP–OIm membranes with different contents of active Co^{II}TPP using the permeation apparatus setup (Fig. S1†) are listed in Table S2.†

The P_{O_2} and P_{N_2} values of the CoTPP–OIm membranes were measured with a single-gas permeation process, and are presented in Fig. 2(a). P_{N_2} remained low and constant regardless of the feed nitrogen pressure. In contrast, P_{O_2} was higher than

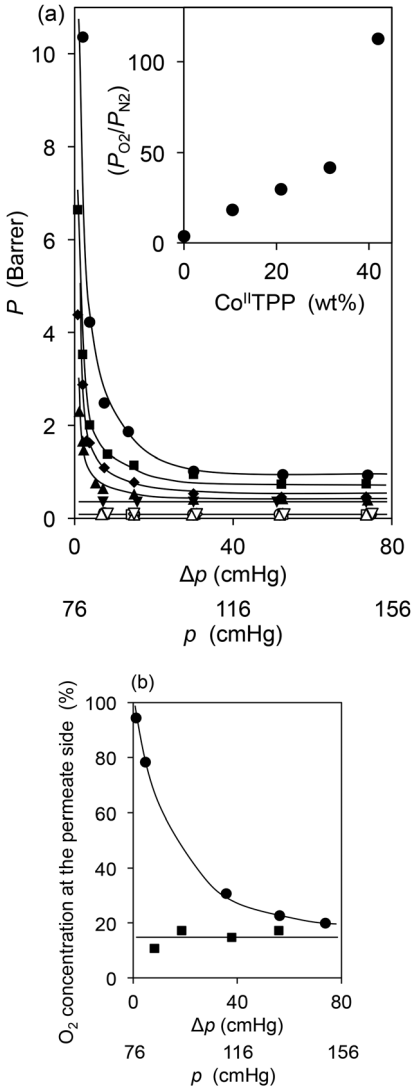

Fig. 2 (a) Single gas permeability coefficients (P) of oxygen and nitrogen at various feed pressures (p) for the CoTPP–OIm membranes. Δp = pressure difference between the feed and permeate sides (Δp = p − atmospheric pressure (76 cmHg)). $Co^{II}TPP$ + $Co^{III}TPP$ = constant 42 wt%. [$Co^{II}TPP$] = 42 (●), 32 (■), 21 (◆), 11 (▲), and 0 (▼) wt%, respectively. The T_g values of the membranes were maintained at *ca.* 6 °C, as summarized in Table S2.† Inset: effect of the active $Co^{II}TPP$ content on O_2/N_2 permselectivity. (b) Oxygen concentration on the permeate side at various air feed pressures for one-shot permeation through the $Co^{II}TPP$–OIm (●) and $Co^{III}TPP$–OIm (■)membranes.

P_{N_2}, and increased steeply as the feed pressure decreased. P_{O_2} achieved 10.4 Barrer at a pressure difference between the feed and permeate side Δp (= p − atmospheric pressure (76 cmHg)) = 2 cmHg, and the oxygen permselectivity P_{O_2}/P_{N_2} reached 113 for the 42 wt% $Co^{II}TPP$ membrane. As shown in the inset of Fig. 2(a), P_{O_2}/P_{N_2} increased with the $Co^{II}TPP$ concentration. P_{O_2} of the $Co^{III}TPP$ membrane (inactive $Co^{III}TPP$ = 42 wt%) was low, even at low feed pressures, and remained constant regardless of the feed pressure. These results indicate that the CoTPP, as the fixed carrier in OIm, facilitates oxygen permeation through the CoTPP–OIm membranes.

3.2. Reversible oxygen interaction and its kinetics with respect to the CoTPP fixed within the polymer membrane under high-pressure or low-temperature conditions

Beforehand, ligation of the imidazole moiety of OIm with $Co^{II}TPP$ was examined with electron spin resonance (ESR) and ultraviolet (UV)–visible spectroscopy. The UV–visible spectrum of the $Co^{II}TPP$ with absorption maxima at 410 nm (Soret band) and 528 nm (Q band) was shifted to 412 nm and 530 nm, respectively, after incorporation into the CoTPP–OIm membrane, which suggests ligation of the imidazole moiety of OIm to CoTPP has taken place. The anisotropy in the ESR spectrum of the CoTPP–OIm membrane in an oxygen-free atmosphere at 77 K suggested that the CoTPP was ligated with OIm and immobilized within the solid-phase polymer. Eight hyperfine structures and three superfine structures in the ESR spectrum were ascribed to the nuclear spin quantum number of divalent cobalt (spin quantum number, I = 7/2) and to the nitrogen nucleus of a single imidazole moiety of OIm ligated to Co^{II}, respectively. Notably, a planar and cavity structure-free CoTPP forms the five-coordinated CoTPP-Im (Im: imidazole moiety). The imidazole ligation only at the fifth coordination site of Co leaves the sixth site vacant to possibly interact with oxygen (eqn (2)).

The selective and reversible interaction reaction of the CoTPP ligated with the imidazole moiety of OIm with an oxygen molecule from air is expressed by:

$$\begin{aligned} &\text{CoTPP-Im} + O_2 \overset{k_{on}}{\rightleftharpoons} O_2\text{-CoTPP-Im} \\ &k_{on}/k_{off} = K = 1/p_{50} \end{aligned} \quad (2)$$

The interaction of the CoTPP fixed in the OIm membrane was measured with visible absorption spectroscopy under a high oxygen pressure using a self-made high-pressure cell (Fig. S3†). The two quartz windows were set in parallel, with the CoTPP–OIm membrane coated on one window facing inside the cell.

The assembly was then carefully sealed under a nitrogen atmosphere. The red-colored membrane yielded a visible absorption spectrum with λ_{max} = 412 nm and 530 nm, attributed to the deoxygenated CoTPP-Im,[29] in the absence of oxygen (Fig. 3(a)). Under high-pressure oxygen gas (0–7 atm) application to the cell, the absorption at 430 nm and 547 nm, attributed to oxygenated CoTPP(Co/O_2 = 1/1 adduct, O_2-CoTPP-Im in eqn (2)), increased with isosbestic points at 420 nm and 535 nm, in response to the oxygen pressure. After degassing inside the high-pressure cell, the CoTPP–OIm spectrum returned to its original deoxygenated form.

The spectral changes in the membrane were also measured at low temperatures with different oxygen partial pressures. The oxygen-binding equilibrium curves obeyed Langmuir isotherms to provide the oxygen-binding affinity p_{50} (the reciprocal of the equilibrium constant (K), the oxygen partial pressure at which half of the CoTPP interacts with oxygen). From the van't Hoff plot or temperature dependence of the logarithmic p_{50}, p_{50} was extrapolated to 920 cmHg for the CoTPP–OIm membrane at 25 °C, as shown in Table 1. The CoTPP-Im in the

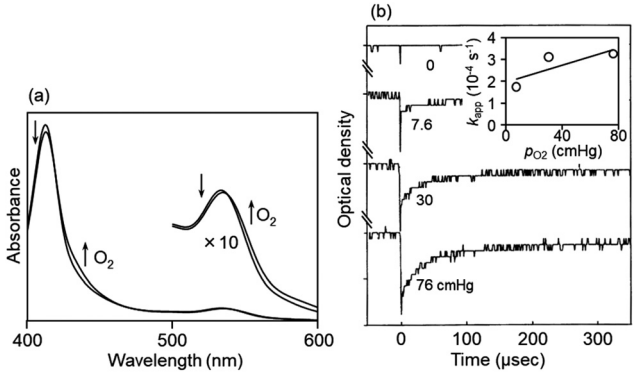

Fig. 3 (a) Visible absorption spectra of the CoTPP–OIm membrane at 25 °C under oxygen at 0 and 7 atm. (b) Absorption recovery at 430 nm after laser flash irradiation at −15 °C, ascribed to the recombination reaction of the photo-dissociated oxygen to the CoTPP complex with OIm in the solid membrane state under an oxygen partial pressure of 0–76 cmHg. Inset: plots of apparent oxygen-binding rate constant (k_{app}) *vs.* oxygen partial pressures at −15 °C.

OIm membrane slightly binds oxygen at room temperature and enables a selective and reversible interaction with oxygen from air.

Photodissociation and recombination of the bound oxygen from and to the CoTPP-Im complex in a cooled OIm membrane were monitored by laser flash photolysis. The laser flash irradiation dissociates the bound oxygen from CoTPP-Im. The oxygen recombination time curve at −15 °C, monitored at the absorption maximum (430 nm) of O_2-CoTPP-Im in eqn (2), is shown in Fig. 3(b), as an example. The spectral change ascribed to the recombination reaction was completed after approximately 100 μs. It was very rapid despite the reaction in the solid-state membrane at low temperature. The plots of the apparent oxygen-binding rate constant (k_{app}) *vs.* applied oxygen partial pressure were linear, which provided the oxygen-binding and oxygen-releasing rate constants (k_{on} and k_{off} in eqn (2)) using pseudo-first-order kinetics, as shown in the inset of Fig. 3(b). From the Arrhenius plots of k_{on} and k_{off}, these values were extrapolated to obtain 5.0×10^7 M^{-1} s^{-1} and 8.6×10^6 s^{-1} at 25 °C, respectively, as shown in Table 1.

The values of p_{50}, k_{on}, and k_{off} extrapolated to 25 °C for the CoTPP-Im fixed within the OIm membrane are listed in Table 1, with those of CoTpivPP[39] (a picketfence porphyrin with a cavity structure on one side of the porphyrin plane, and benchmark cobaltporphyrin to reversibly bind an oxygen molecule at room temperature from air), also fixed within the OIm membrane. Compared to the values for the CoTpivPP in the membrane, p_{50} was as high as 920 cmHg (1.23 MPa) with extremely weak interaction with oxygen and the k_{off} was significantly larger in the two digits for the CoTPP–OIm membrane. The CoTPP-Im is kinetically very active when interacting with oxygen. The significantly large oxygen-releasing rate constant results in an extremely low oxygen-binding affinity. These results indicate that the very small oxygen-binding affinity and extremely rapid release of oxygen from the CoTPP fixed within the OIm membrane are potentially the key factors for high oxygen permeability with high P_{O_2}/P_{N_2}.

Table 1 The oxygen partial pressure at which half of the cobaltporphyrin interacts with oxygen (p_{50}), and the oxygen-binding and releasing rate constants (k_{on} and k_{off}) of the cobaltporphyrin–OIm membranes extrapolated to 25 °C

Cobaltporphyrin	p_{50} (cmHg)	10^{-7} k_{on} (M^{-1} s^{-1})	10^{-4} k_{off} (s^{-1})
CoTPP	920	5.0	860
CoTpivPP[29]	7.6	1.7	1.2

3.3. Diffusivity and solubility of oxygen in the CoTPP–OIm membranes

According to oxygen sorption measurement, the oxygen sorption amount in the CoTPP–OIm membrane at 78 cmHg was 0.70 cm^3 (STP) cm^{-3}. This provided the molar ratio [dissolved oxygen]/[CoTPP] = *ca.* 1/20 for the 42 wt% CoTPP membrane even under 78 cmHg at 25 °C. In addition, a very large p_{50} (or very weak oxygen-binding affinity) of the CoTPP for the oxygen interaction indicates that the number of CoTPP molecules bound with oxygen is less than one in 1000 even at an oxygen pressure of 76 cmHg. These results imply that most of the oxygen molecules in the membrane are physically dissolved. Their amount is considerably smaller than the amount of the CoTPP in the membrane under the conditions when the facilitated oxygen permeation was observed.

The Damköhler number[41] (Ψ), expressed by eqn (3), is one of the nondimensional parameters used to compare the diffusivity *via* a chemical reaction and physical diffusivity:

$$\Psi = (k \cdot L^2/D) \quad (3)$$

where L is the membrane thickness, D is the physical diffusion coefficient, and k is the first-order rate constant of the reaction, *i.e.*, k_{off}, the oxygen-releasing rate constant in this study. D for the CoTPP–OIm membrane was estimated with the oxygen sorption amount and permeability coefficient of the 42 wt% Co^{III}TPP-OIm membrane to be 7.6×10^{-8} cm^2 s^{-1}. With these values, Ψ was calculated to be 7300, which implies that the chemical diffusion *via* the CoTPP as a fixed carrier in the membrane is significantly larger compared to the physical diffusion through the membrane. The temperature dependences of P_{O_2} and P_{N_2} for the 42 wt% Co^{II}TPP-OIm membrane were compared to those of the corresponding inactive Co^{III}TPP-OIm membrane, and are presented by $\ln(P_{N_2})$ *vs.* $1/T$ or Arrhenius plots in Fig. 4. The membrane is significantly larger compared to the physical diffusion through the membrane. The activation energy (E_a) values for nitrogen permeation were 12 and 13 kJ mol^{-1} for the Co^{II}TPP and the Co^{III}TPP membranes, respectively. E_a for oxygen permeation through the control Co^{III}TPP membrane was 9 kJ mol^{-1}, slightly lower than that of nitrogen permeation, which was not inconsistent with the physical permselectivity of P_{O_2}/P_{N_2} = 3.7 for the membrane. On the other hand, E_a of P_{O_2} for Co^{II}TPP was 24 kJ mol^{-1} and significantly higher than those values for the physical permeation

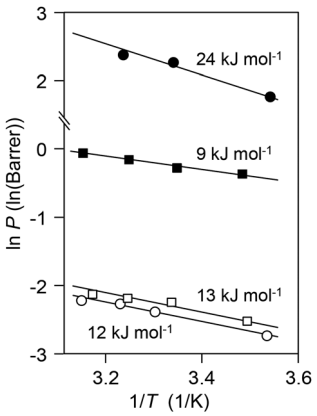

Fig. 4 Arrhenius plots of P_{O_2} (solid symbols) and P_{N_2} (open symbols) for the Co^{II}TPP–OIm (circle) and Co^{III}TPP–OIm (square) membranes.

of oxygen through the Co^{III}TPP membrane and of nitrogen through the Co^{II}TPP and Co^{III}TPP membranes. This result supports the contribution of the chemical reaction of the CoTPP fixed within the membrane, in addition to the physical permeation process, for the facilitated oxygen permeation. The distance of the CoTPP fixed within the OIm membrane was estimated with the size of the CoTPP molecule (approximately 1.3 nm). For the 42 wt% CoTPP membrane, the CoTPP molecules are in contact with each other and approximately 60 CoTPPs are packed and aligned in the direction of the membrane with a thickness of approximately 80 nm.

The above results conclude that the oxygen dissolved in the membrane is mainly due to a physical dissolution, and additionally that the CoTPP, condensedly fixed in the membrane, selectively but very kinetically interacts with oxygen with an extremely high oxygen-releasing rate, and contributes to the significantly facilitated oxygen permeation through the membrane.

3.4. Oxygen permeability and enrichment from dry air using enlarged CoTPP–OIm membranes

For practical separation, dry air, a mixture of O_2 and N_2, is applied as feed gas to examine oxygen enrichment with a single permeation pass through the CoTPP–OIm membrane, using the 42 wt% Co^{II}TPP-OIm membrane and corresponding Co^{III}TPP membrane as a control. The experimental setup for the measurement is illustrated in Fig. S1,† while the oxygen concentration on the permeate side was analyzed with gas chromatography using helium as a carrier gas. Fig. 2(b) shows the permeate oxygen concentration at various air feed pressures (p). The oxygen concentration through the Co^{III}TPP-OIm membrane remained low and constant regardless of the air feed pressure. In contrast, the permeated oxygen concentration increased as the air feed pressure decreased, and the oxygen concentration reached 94% with a flow rate of 0.48 cm^3 (STP) cm^{-2} min^{-1} at p = 78.3 cmHg. The oxygen concentration on the permeate side was calculated to be 98% based on the single-gas P_{O_2} and P_{N_2} in the previous section, which almost coincided with the oxygen enrichment performance from air using the same CoTPP–OIm membrane.

The CoTPP–OIm membrane with a larger area was prepared to support the oxygen enrichment result from air. Employing the same process as used for the smaller membrane, a pinholeless CoTPP–OIm-coated membrane with a diameter >10 cm was prepared, as shown in Fig. 5(a). Permeation apparatus for the CoTPP–OIm membrane with a surface area of 80 cm^2 was designed to evaluate the gas permeability, as shown in Fig. 5(b) and (c). The feed side volume was set to a value as large as possible (>700 cm^3), and a fan was placed inside the

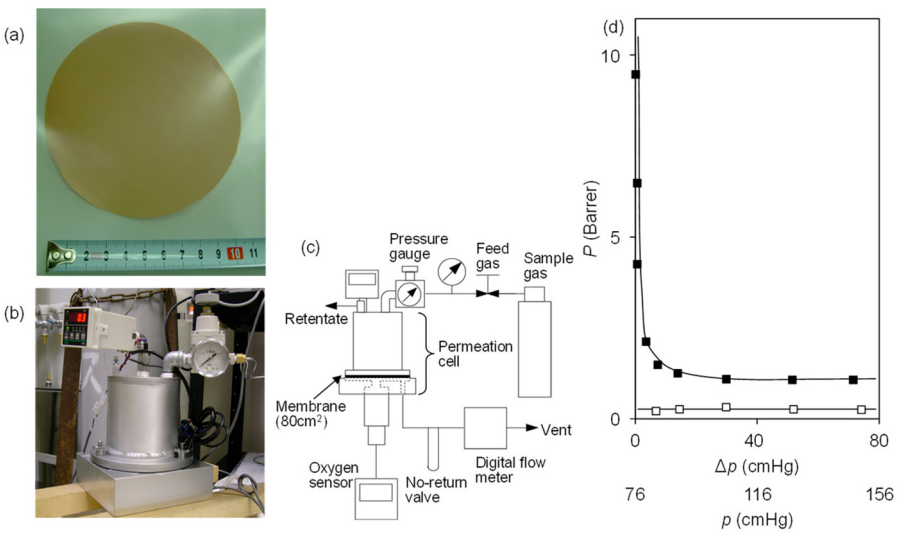

Fig. 5 (a) The CoTPP–OIm membrane for permeability measurement (10 cm diameter). (b) Photograph of the apparatus used for permeability measurements. (c) Flow diagram with oxygen sensor for the permeability measurements of larger size; the feed chamber size is >700 cm^3, and the permeate chamber is *ca.* 50 cm^3. (d) Single gas permeability coefficients of O_2 (solid squares) and N_2 (open squares) at various feed pressures for the CoTPP–OIm membrane of 10 cm diameter. Δp = pressure difference between feed and permeate side ($\Delta p = p$ – atmospheric pressure (76 cmHg)).

Table 2 Oxygen concentrations at the permeate side [O_2] at various feed pressures of dry air for the Co^{II}TPP–OIm and Co^{III}TPP–OIm membranes with large 10 cm diameter. Δp = pressure difference between feed and permeate side ($\Delta p = p$ − atmospheric pressure (76 cmHg))

Co^{II}TPP	Δp (p) (cmHg)	2 (78)	4 (80)	8 (84)	48 (124)	76 (152)
	[O_2] (%)	61	62	49	38	38
Co^{III}TPP	Δp (p) (cmHg)			15 (91)	53 (129)	76 (152)
	[O_2] (%)			35	36	35

feed side room to maintain the oxygen concentration of the air feed constant during the permeation experiment. The volume of the permeation side was minimized to approximately 50 cm^3 to sweep the permeated gas immediately to minimize back permeation. The permeate gas was monitored with the accommodated bubble flow meter and fluorescent oxygen sensor. The P_{O_2} and P_{N_2} values using single gases in this permeation process were measured, in advance, and compared with the results obtained for the previous smaller membrane, as shown in Fig. 5(d). The P_{N_2} value of the large membrane was almost the same as that of the smaller membrane, which indicates the validity of this permeation measurement. The P_{O_2} value was larger than that for P_{N_2} and rapidly increased with the decreasing feed pressure, reaching 9.5 Barrer at Δp of 1 cmHg and P_{O_2}/P_{N_2} permselectivity of 50. These results indicate that facilitated oxygen permeation through the CoTPP–OIm membrane was observed even when using the membrane with a large area.

The oxygen concentrations detected on the permeate side through the Co^{II}TPP–OIm and Co^{III}TPP–OIm membranes for dry air application under pressure are summarized in Table 2. For the Co^{III}TPP membrane, the oxygen concentration remained low and was unaffected by the air feed pressure. On the other hand, the oxygen concentration definitely increased as the air feed pressure decreased for the Co^{II}TPP membrane permeation. An oxygen enrichment of approximately 60% was observed at an additional pressure of 2 cmHg at the air feed side with a flow rate of 60 mL min^{-1} m^{-2}.

The P_{O_2} and P_{O_2}/P_{N_2} values measured for the CoTPP–OIm membrane in this study are extremely high, in comparison with those reported for polymer membranes[42] (Fig. S4†).

4. Conclusions

P_{O_2} reached 10 Barrer with high oxygen permselectivity P_{O_2}/P_{N_2} > 110. The attained oxygen enrichment from air value was approximately 60% for the polymer membrane of OIm ligated with the simple and planar 42 wt% CoTPP. This significantly facilitated oxygen permeation through the membrane as discussed, with the selective but very kinetic oxygen interaction of the CoTPP carrier having an extremely high oxygen-releasing rate constant.

In addition, the CoTPP–OIm membrane was flexible and durable and was facile for preparation and scale-up in size. These features are promising for the membrane when testing in medical applications, air batteries, and other scenarios where oxygen-enriched air is needed.

Author contributions

H. S. and H. A. performed the experimental work and H. S. and H. N. prepared the manuscript.

Data availability

The data supporting this article have been included as part of the ESI.† Data are available upon reasonable request from the authors.

Conflicts of interest

There are no conflicts to declare.

Acknowledgements

This work was supported by KAKENHI from the Ministry of Education, Culture, Sports, Science and Technology, Japan.

References

1 Y. Yampolskii, *Macromolecules*, 2012, **45**, 3298–3311.
2 D. F. Sanders, Z. P. Smith, R. Guo, L. M. Robeson, J. E. McGrath, D. R. Paul and B. D. Freeman, *Polymer*, 2013, **54**, 4729–4761.
3 S. Hasebe, S. Aoyama, M. Tanaka and H. Kawakami, *J. Membr. Sci.*, 2017, **536**, 148–155.
4 R. S. K. Valappil, N. Ghasem and M. Al-Marzouqi, *J. Ind. Eng. Chem.*, 2021, **98**, 103–129.
5 K. Cheng, K. Shinohara, O. Notoya, M. Teraguchi, T. Kaneko and T. Aoki, *Sep. Purif. Technol.*, 2024, **20**, 2308050.
6 H. Nishide, *Green Chem.*, 2022, **24**, 4650–4679.
7 H. Shinohara and H. Nishide, *Polym. Adv. Technol.*, 2024, **35**, e6524.
8 R. S. Murali, T. Sankarshana and S. Sridhar, *Sep. Purif. Technol.*, 2013, **42**, 130–186.
9 *Polymer Handbook*, ed. J. Brandrup and E. H. Immergut, 3rd edn, Wiley-Interscience, New York, 1989.
10 W. J. Koros and C. Zhang, *Nat. Mater.*, 2017, **16**, 289–297.
11 T. Sakaguchi, Y. Hu and T. Masuda, in *Membrane Materials for Gas and Vapor Separation*, ed. Y. Yampolskii and E. Finkelshtein, John Wiley & Sons, Ltd, 2017, pp. 107–142.

12 A. Figoli, W. F. C. Sager and M. H. V. Mulder, *J. Membr. Sci.*, 2001, **181**, 97–110.
13 A. Matsuoka, E. Kamio, T. Mochida and H. Matsuyama, *J. Membr. Sci.*, 2017, **541**, 393–402.
14 P. Luangrujiwong, A. Sungpet, J. D. Way and R. Jiraratananon, *Ind. Eng. Chem. Res.*, 2006, **45**, 8213–8216.
15 W. J. Koros, Y. H. Ma and T. Shimidzu, *Pure Appl. Chem.*, 1996, **68**, 1479–1489.
16 H. Nishide, M. Ohyanagi, O. Okada and E. Tsuchida, *Macromolecules*, 1986, **19**, 494–496.
17 H. Nishide, M. Ohyanagi, O. Okada and E. Tsuchida, *Macromolecules*, 1987, **20**, 417–422.
18 H. Nishide, T. Suzuki, H. Kawakami and E. Tsuchida, *J. Phys. Chem.*, 1994, **98**, 5084–5088.
19 H. Nishide, Y. Tsukahara and E. Tsuchida, *J. Phys. Chem. B*, 1998, **102**, 8766–8770.
20 B. Shentu and H. Nishide, *Ind. Eng. Chem. Res.*, 2003, **42**, 5954–5958.
21 E. Tsuchida, H. Nishide, M. Ohyanagi and H. Kawakami, *Macromolecules*, 1987, **20**, 1907–1912.
22 W. Choi, P. G. Ingole, H. Li, S. Y. Park, J. H. Kim, H.-K. Lee and I.-H. Baek, *Microchem. J.*, 2017, **132**, 36–42.
23 S. Sunderrajan, B. D. Freeman, C. K. Hall and I. Pinnau, *J. Membr. Sci.*, 2001, **182**, 1–12.
24 J. H. Kim, B. R. Min, C. K. Kim, J. Won and Y. S. Kang, *Macromolecules*, 2002, **35**, 5250–5255.
25 J. H. Kim, B. R. Min, J. Won, S. H. Joo, H. S. Kim and Y. S. Kang, *Macromolecules*, 2003, **36**, 6183–6188.
26 C. Yu, M. G. Cowan, R. D. Noble and W. Zhang, *Chem. Commun.*, 2014, **50**, 5745–5747.
27 J. P. Jung, C. H. Park, J. H. Lee, J. T. Park, J.-H. Kim and J. H. Kim, *J. Membr. Sci.*, 2018, **548**, 149–156.
28 N. U. Kim, J.-H. Kim, B. R. Park, K. C. Kim and J. H. Kim, *J. Membr. Sci.*, 2021, **620**, 118939.
29 H. Shinohara, T. Arai and H. Nishide, *Macromol. Symp.*, 2002, **186**, 135–139.
30 H. Shinohara, A. Nakao and H. Nishide, *Kobunshi Ronbunshu*, 2002, **59**, 656–660.
31 H. Shinohara, H. Shibata, D. Wöhrle and H. Nishide, *Macromol. Chem. Phys.*, 2005, **26**, 467–470.
32 N. Preethi, H. Shinohara and H. Nishide, *React. Funct. Polym.*, 2006, **66**, 851–855.
33 M. Shoji, K. Oyaizu and H. Nishide, *Polymer*, 2008, **49**, 5659–5664.
34 N. Chikushi, E. Ohara, A. Hisama and H. Nishide, *Macromol. Rapid Commun.*, 2014, **35**, 976–980.
35 H. Nagar, P. Vadthya, N. S. Prasad and S. Sridhar, *RSC Adv.*, 2015, **5**, 76190–76201.
36 H. Li, W. Choi, P. G. Ingole, H. K. Lee and I. H. Baek, *Fuel*, 2016, **185**, 133–141.
37 E. Tsuchida and H. Nishide, *Top. Curr. Chem.*, 1986, **132**, 63–99.
38 *Metal Complexes and Metals in Macromolecules: Synthesis, Structure and Properties*, ed. D. Wöhrle and A. D. Pomogailo, Wiley-VCH GmbH, Weinheim, 2003.
39 J. P. Collman, R. R. Gagne, C. Reed, T. R. Halbert, G. Lang and W. T. Robinson, *J. Am. Chem. Soc.*, 1975, **97**, 1427–1439.
40 J. P. Collman, J. I. Brauman, K. M. Doxsee, T. R. Halbert, S. E. Hayes and K. S. Suslick, *J. Am. Chem. Soc.*, 1978, **100**, 2761–2766.
41 C. Weiland, in *Mechanics of Flow Similarities*, ed. C. Weiland, Springer, Cham, 2020, pp. 39–50.
42 L. M. Robeson, *J. Membr. Sci.*, 2008, **320**, 390–400.